Design and characterization of zero magnetic field chambers for high efficiency neutron polarization transport

Dadisman, Ryan; Shen, Jiazhou; Feng, Hao; Crow, Lowell; Jiang, Chenyang; Wang, Tianhao; Zhang, Yuxuan; Bilheux, Hassina; Parnell, Steven R.; More Authors

DOI
10.1016/j.nima.2019.05.092

Publication date
2019

Document Version
Accepted author manuscript

Published in
Nuclear Instruments and Methods in Physics Research, Section A: Accelerators, Spectrometers, Detectors and Associated Equipment

Citation (APA)
Dadisman, R., Shen, J., Feng, H., Crow, L., Jiang, C., Wang, T., Zhang, Y., Bilheux, H., Parnell, S. R., & More Authors (2019). Design and characterization of zero magnetic field chambers for high efficiency neutron polarization transport. *Nuclear Instruments and Methods in Physics Research, Section A: Accelerators, Spectrometers, Detectors and Associated Equipment*, *940*, 174-180. https://doi.org/10.1016/j.nima.2019.05.092

Nuclear Inst. and Methods in Physics Research, A xxx (xxxx) xxx

Contents lists available at ScienceDirect

Nuclear Inst. and Methods in Physics Research, A

journal homepage: www.elsevier.com/locate/nima

Design and characterization of zero magnetic field chambers for high efficiency neutron polarization transport

Ryan Dadisman [a], Jiazhou Shen [b], Hao Feng [b], Lowell Crow [a], Chenyang Jiang [a], Tianhao Wang [a], Yuxuan Zhang [a], Hassina Bilheux [a], Steven R. Parnell [c], Roger Pynn [a,b], Fankang Li [a,*]

[a] Neutron Sciences Directorate, Oak Ridge National Laboratory, Oak Ridge, TN 37830, USA
[b] Center for Exploration of Energy and Matter, Indiana University, Bloomington, IN 47408, USA
[c] Faculty of Applied Sciences, Delft University of Technology, Mekelweg 15, Delft, JB 2629, Netherlands

ARTICLE INFO

Keywords:
Magnetic Wollaston prisms
Larmor labeling
Large-angle neutron scattering
Small-angle neutron scattering
Zero magnetic field
Polarization transport

ABSTRACT

Several methods of polarized neutron scattering call for a zero magnetic field (ZF) region to reduce magnetic field integral aberrations while preserving the neutron polarization. Though the design for large angle neutron scattering has been presented in various places, the design characterization and tuning has not been discussed before. In this report, the tuning procedure will be discussed with both neutron polarization transport method and utilization of fluxgate magnetometers. As a tuning procedure, polarized neutrons are sensitive to any local field distortions along all trajectories within the beam, but the process is slow. With fluxgates, the entire beam region cannot be accessed simultaneously, but very fast and precise measurements can be made in accessible regions of interest. Consequently, we would like to benchmark the usage of fluxgates as a fast tuning probe compared with polarization measurements made with neutrons. Polarization transport results for tuned ZF chambers, up to 2.25 m in length, are presented.

1. Introduction

Methods which utilize the precession of the neutron spin in a well designed magnetic field enable the investigations of material structures or dynamics with a resolution beyond the conventional neutron scattering techniques. Mezei proposed the first technique of this type, neutron spin echo (NSE) [1], which was further developed into neutron resonance spin echo (NRSE) [2], modulated intensity with zero effort (MIEZE) [3], spin echo small angle neutron scattering (SESANS) [4] and spin echo modulated small angle neutron scattering (SEMSANS) [5]. NRSE uses radio frequency (RF) flippers to measure the excitations of quasiparticles, for example, phonon or magnon and MIEZE only uses one arm of NRSE to allow more relaxed sample environment. Similar to the relation between NRSE and MIEZE, SESANS and SEMSANS employ magnetic Wollaston prisms to measure the inter particle correlations of materials in a extended length scale.

Since all of these methods label the change in either neutron energy (E) or momentum transfer (Q) into a change in Larmor phase, i.e., the accumulated angle of neutron spin precession, they may be referred as neutron Larmor labeling techniques. To maximize the resolution of a small change in either E or Q, it is critical to maximize the achievable Larmor phase, $\Phi \propto FI \times \lambda$, where FI is the magnetic field integral along the neutron path and λ is the neutron wavelength. From this it follows that maximizing the Larmor phase requires maximizing the magnetic field, path length of neutron, or neutron wavelength. To achieve a high signal to noise ratio for a given setup, the Larmor phase aberrations need to be minimized across the beam. To maximize the resolution while maintaining a high signal to noise ratio, one approach is to introduce the usage of zero magnetic field (ZF) chamber to separate the spin manipulation components far apart from each other, where the neutron polarization vector will be preserved when passing through this region without accumulating additional Larmor phase. This is especially true for the techniques involving resonance radio frequency flippers, such as NRSE or MIEZE, where an effective precession is produced inside the ZF chamber such that the accumulated phase is proportional to the time neutrons spend between and the angular frequency of the flippers. This is also true for methods using static magnetic fields, such as SESANS or SEMSANS, where the gradient of the field integral inside the spin manipulation devices matters for the Larmor phase. It is true that people can also use well designed uniform magnetic guide field to preserve the neutron polarization [6]. But careful shielding of this field is critical at the magnetic field boundary where one does not need it, for example, a $\pi/2$ spin flipper.

Another situation where a ZF chamber is preferable originates from the fact that a uniform Larmor phase across the sample is essential, especially for large angle scattering on a sample with finite size, i.e., a diffraction setup. Introducing ZF chambers in the regions where spin

* Corresponding author.
E-mail address: fankangli@hotmail.com (F. Li).

https://doi.org/10.1016/j.nima.2019.05.092
Received 21 December 2018; Received in revised form 28 May 2019; Accepted 29 May 2019
Available online xxxx
0168-9002/

precession is not desired is one approach to achieve this, though care must be taken to preserve the neutron polarization vector.

One of the recent developments in Larmor labeling methods is the introduction of superconducting magnetic Wollaston prisms [7]. Such devices are composed of pairs of triangular shaped magnetic field regions using superconducting coils. These adjacent regions of field are opposite in direction and both transverse to the beam direction, and by using superconducting films at the interfaces, the magnetic field is very uniform and well defined within the regions. The angle between the interface of the opposite fields and the beam direction introduces a splitting of the spin states at the interface in a beam which is polarized perpendicular to the fields. Wollaston prisms can be applied for large angle neutron scattering, including neutron Larmor diffraction [8,9] and inelastic neutron scattering spectroscopy [10]. In such applications, a sample with finite size will lead to a variation of the neutron path length introducing Larmor phase aberrations in a uniform magnetic field. A ZF chamber with high efficiency polarization transport is essential in the sample region, i.e., between the precession devices, so that the Larmor phase accumulation is controlled purely by the precession devices. Such prisms have also been used to implement SEMSANS for small angle scattering, in which a long separation between the spin flippers yields longer spin echo lengths and the span should have ZF to prevent additional phase accumulation. In this report, we discuss the design and characterization of the ZF chamber for both large and small angle applications, and discuss the benefits of using magnetometry as a fast method of optimizing compensation coils for ZF chambers, which could also be used for other techniques.

2. The ZF chamber for large angle neutron scattering technique

2.1. The design of the ZF chamber

The ZF chamber used in MuPAD [11], a spherical neutron polarimeter at the Paul Scherrer Institut (PSI) triple axis spectrometer, and NRSE of FRM-II [12–14] consists of three components: a cylindrical ZF chamber with a gap in the middle at the sample height; and two rectangular mu metal boxes with beam port open ends to magnetically shield the gaps between the central ZF chamber and the precession devices. As shown in Fig. 1, the design presented here is similar to those used for MuPAD and NRSE. Differently, the gap between the top and bottom mu metal cylinder is closed by an inner concentric mu metal cylinder. Two beam ports on the sides of the cylinder are provided to allow the beam to pass through, as shown in Fig. 1(a). The inner cylinder is configured such that the two beam ports will remain open when rotating the scattering ARM-II. The two mu metal boxes surrounding the Wollaston prisms are then connected to the two beam ports to optimize the shielding efficiency. As a rule of thumb, the size of the ports needs to be optimized; a larger port will have a lower shielding factor, while a smaller port will limit the beam size.

An open ended cylindrical shield is most effective at attenuating the components of the magnetic field which are transverse to its longitudinal axis. Consequently, the longitudinal component of the ambient magnetic field, i.e., the component normal to the top and bottom, will be the dominant stray field to enter the sample region, as shown in Fig. 1(a) and 2. Rather than closing the open ends to fully shield the sample environment, compensation coils placed on the top and bottom provide more flexibility to cancel the stray fields entering the region while allowing access for sample environment equipment, e.g., a cryostat. For the two ports where the beam is passing through, compensation coils are also used here to further reduce the stray fields along the beam. These features are similar to what has previously been used in MuPAD [11] and NRSE [12–14].

This concentric shell design was simulated using MagNet [15] finite element analysis software. The zero-angle configuration was simulated, i.e., the left and right ports are directly aligned and this will result in a hole in the shield shown in Fig. 1. This represents the worst possible

(a)

Nutator

Please cite this article as: R. Dadisman, J. Shen, H. Feng et al., Design and characterization of
Inst. and Methods in Physics Research, A (2019), https://doi.org/10.1016/j.nima.2019.05.09

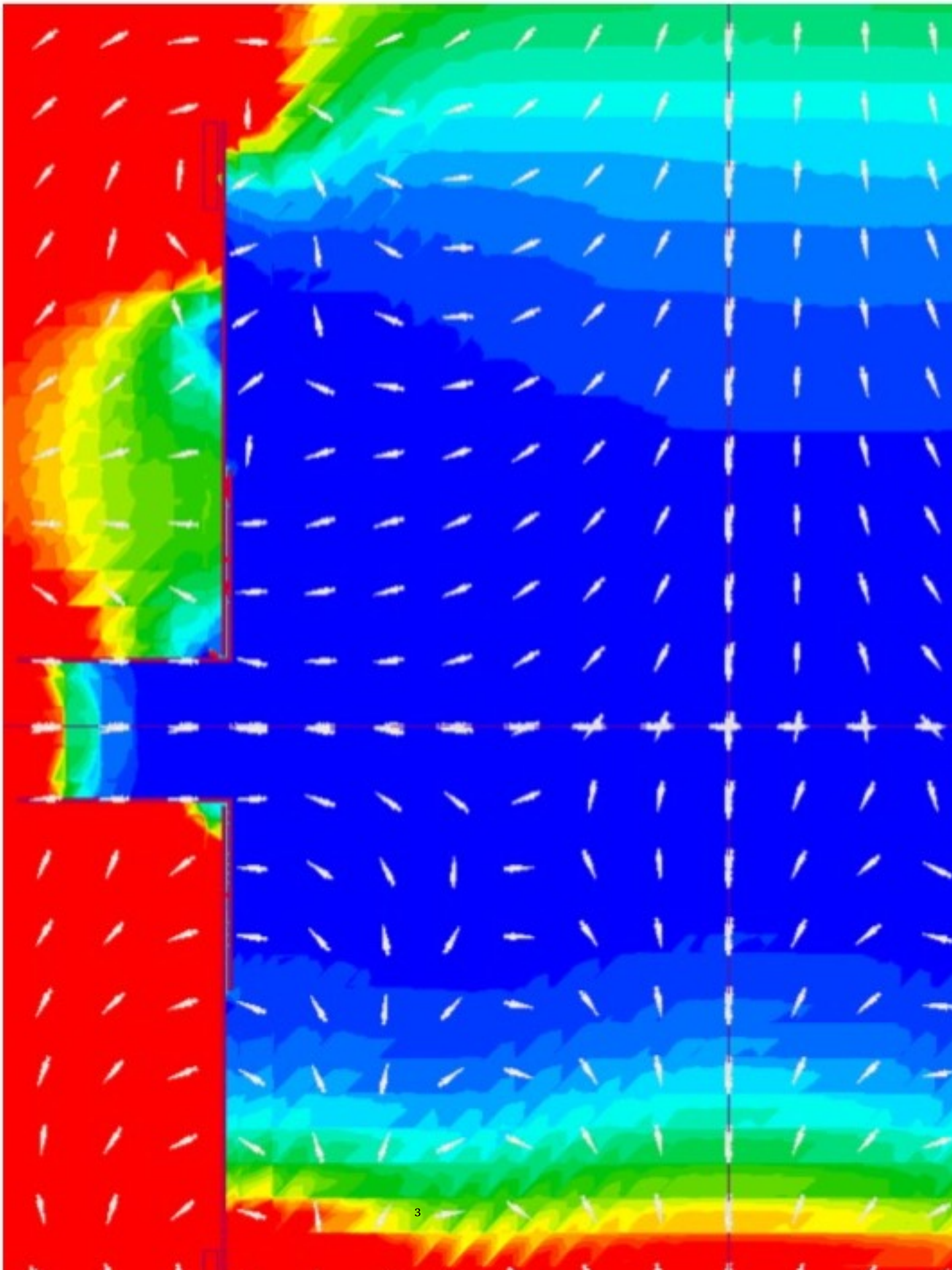

configuration for the ZF chamber because at larger angles the gap will be eliminated due to the rotation of the inner mu metal cylinder. Exterior Helmholtz coils are used to simulate the expected ambient background field, which is ~10 Gauss at the sample region caused by the magnetized goniometer of the beamline. Simulation results, as given in Fig. 2, shows that any magnetic flux that is transverse to the ZF chamber will be shielded and the residual component parallel to the openings can be canceled using compensation coils. As shown in Fig. 2(b), the hole produced by the concentric shields not overlapping at low angles is not compensated, but it has a minimal effect on the magnetic field at the beam and sample locations. The overlapping concentric shell design will further reduce the flux leakage through this hole substantially, resulting in very good field attenuation along the beam line.

2.2. The tuning and compensation coils of the ZF chamber

There are two methods we can use to tune the compensation coils: using a fluxgate magnetometer to minimize the field readings; and maximizing the polarization efficiency with a polarized neutron beam. The reason to compare the two methods is due to the time required to perform these two methods, which will be discussed later in this report. Since there are four coils involved, a clear strategy is important, which will be presented here. For both methods, the first step is always to tune the top and bottom coils, after which their settings will be fixed for the following tuning. It is important to tune the top and bottom coils first since they will also contribute the most stray field to the central sample region and will also produce stray fields inside the two ports. For the two ports, there are three sources of stray field: from the top and bottom compensation coils, shown in Fig. 1(a); external ambient stray field; and the neighboring superconducting Wollaston prisms. Please note that the field here might be high (a couple of G) due to the flux concentration of the surrounding mu metal. The first two contributions are constant but the contribution from the prism scales with the current within the prism's coils. Consequently the compensation coils inside the two ports need to be tuned for each prism current setting.

For this experiment, the fluxgate magnetometer tuning procedure is simply to tune the current inside the coils such that the stray field is less than 0.01G measured at a fixed spot inside each port, using a Bartington Mag-01H magnetometer. Any stray magnetic fields inside the ports will interact with the neutron polarization vectors thus leading to low polarization transfer efficiency when neutrons are passing through the whole setup in Fig. 1. The tuning procedure using neutron polarization in this case is to optimize the polarization efficiency by scanning the compensation current inside the left and right coils, saving time by using the top and bottom compensation coil settings found via magnetometry. Additionally, rather than measuring the full polarization with two spin states measurements, only one spin state was used. When the polarization transport is maximized, it would yield a global maximum or minimum neutron count per unit time, depending on the experimental setup.

The experiment was conducted on HB-2D beam line [16] at the High Flux Isotope Reactor (HFIR) of Oak Ridge National Laboratory using 4 Å neutrons. To measure the polarization transfer efficiency, the apparatus was set up with the fields inside the two nutators aligned parallel to the magnetic field vectors inside the prisms ($\pi - \pi$ mode). In this situation, only the ZF chamber contributes to the variation of the polarization transfer when we are tuning the compensation coils. The compensation tuning with neutrons was performed with each coil separately, in which the coil not being tuned was turned off. A comparison of the compensation current inside the two coils found via neutron measurement and magnetometry has been plotted in Fig. 3 for different currents inside the prisms. Please note that the field inside the prisms has been set such that they are all parallel to each other; the field inside the ARM-I and ARM-II prisms are opposite to each other with the same field intensity. Clearly, for both methods, the trend of

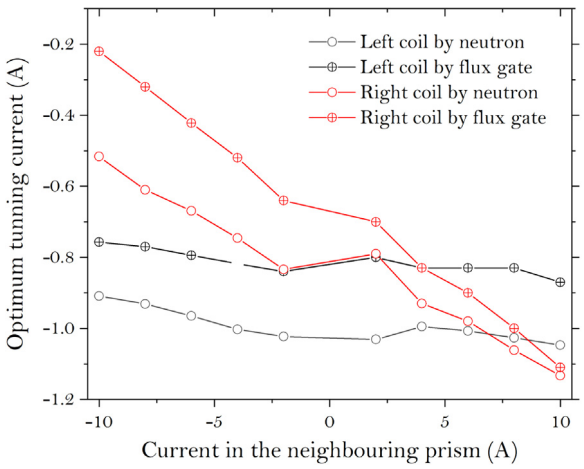

Fig. 3. The tuning curve of the left and right compensation coils on the two ports in Fig. 1 as a function of current inside the two prisms. The black and red lines denote the left and right compensation coils respectively. (For interpretation of the references to color in this figure legend, the reader is referred to the web version of this article.)

the tuning curve agrees with each other, though the optimum current in the compensation coils obtained by neutron polarization is always lower than that of the one by fluxgate. The reason is that the fluxgate, inserted into the port from the ZF chamber side, is ~ 2.5 cm away from the prism due to the vacuum chamber surrounding it, which prevents accurate minimization of the field just outside the prism.

To understand how the tuning will contribute to our actual neutron measurements, the polarization efficiency is measured by setting the nutator field perpendicular to the field inside the prisms ($\pi/2 - \pi/2$ mode). In this mode, the neutron polarization vector will start to precess around the magnetic field vectors inside the prisms. Therefore the neutron will accumulate a Larmor phase inside ARM-I which will be mostly canceled in ARM-II as in neutron spin echo [17], since they always have the same magnitude but opposite directed magnetic field. The polarization efficiency is obtained by sweeping the current inside ARM-II about the current set in ARM-I, for both methods of tuning. To demonstrate the necessity of optimizing the compensation coils for each prism current setting, we performed an "off-tune" measurement by fixing only the right compensation coil constant at the optimum for 2 A inside the neighboring prism, then tested it with different prism settings. As shown in Fig. 4, the results given by either fluxgate or neutrons are very close, so that we can use the fluxgate method as a fast way of tuning the compensation coil in the two ports. However, when the right compensation coil is off-tune for high prism current, some depolarization occurs indicating that the compensation must be exactly performed for each prism setting. It should be noted that the measurement in Fig. 4 does not represent the worse situation, where the left compensation coil is still optimized to each prism current, and the prisms is only operating in a low current far below its routine operational current (50 A). Additionally, a NRSE setup with a ZF tube in each arm and a ZF chamber around the sample would have 6 port compensation coils, so that even a small loss of polarization at each port will compound to substantial depolarization. The necessary act of re-tuning the compensation coils when the prism settings are changed provides further support for the faster method using magnetometry.

2.3. Characterization of the ZF chamber with an off-tune compensation coil

So now the question becomes what happens if the compensation coil is not completely on-tune and how much stray field can be tolerated. To investigate this, the setup shown in Fig. 1(a) was used with the field of the first nutator aligned parallel to the prism field and the second nutator aligned perpendicular to the prism field ($\pi - \pi/2$ mode). In this

Please cite this article as: R. Dadisman, J. Shen, H. Feng et al., Design and characterization of zero magnetic field chambers for high efficiency neutron polarization transport, Nuclear Inst. and Methods in Physics Research, A (2019), https://doi.org/10.1016/j.nima.2019.05.092.

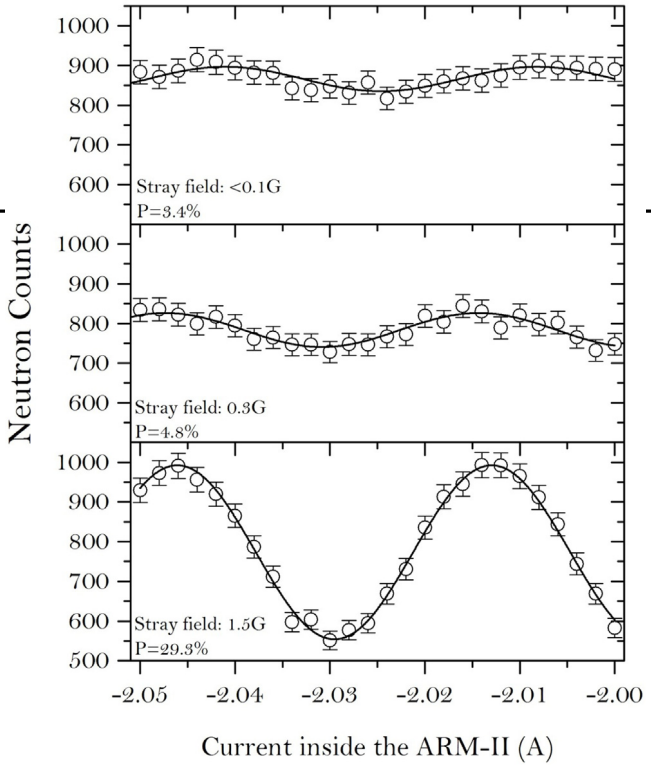

Fig. 5. The oscillations obtained by scanning the current inside ARM-II with the nutator fields orthogonal to each other, so that nominally no polarization should be transmitted. The observed increase in oscillation amplitude with increasing field inside the ZF chamber indicates more depolarization in the region. Data fitted to a simple sinusoid function to determine the polarization.

Fig. 4. The polarization efficiency, as a function of prism current, obtained with the tuning current optimized using neutrons (red circle) and a fluxgate magnetometer (black square). The measurement with the right compensation coil off-tune (blue diamond) is presented for comparison. For these three measurements, the left compensation coil is always optimized for each prism current. The damping of the polarization with the compensation coil on tune (red circle and black square) is due to the residual magnetic field of the iron pole pieces, which will introduce inhomogeneous field integral across the beam. This can be fixed and improved by properly degaussing all the iron pole pieces inside the device.

case, if the ZF chamber is perfect, we expect to observe no polarization at the detector since there is no projection from a vertically orientated polarization vector (defined by the first nutator) into a horizontal plane defined by the second nutator. In this way, we are able to measure how much of the neutron polarization vector has been kicked out of its principal axis into the horizontal plane, i.e., depolarized, due to remnant ambient magnetic fields.

To measure the polarization efficiency of the principal precession axis, the current inside of ARM-II was scanned, as shown in Fig. 5, with various settings of stray field inside the right port. As measured by the fluxgate, when there is no stray field present, there are still some measurable oscillations. Again, this means the polarization vector of some of the neutrons is kicked out of its principal precession axis, defined by the first nutator, when going through the ZF chamber. As the stray field increases, the oscillations become clearer, which will introduce more depolarization. But with a stray field of 0.3G shown in the middle plot of Fig. 5, the polarization is almost the same as that of the ZF (top plot of Fig. 5). So in subsequent experiments involving the ZF chamber, it is routinely operated with a stray field of less than 0.1G.

3. The ZF chamber for low angle neutron scattering technique

The SEMSANS method employs two magnetic Wollaston prisms separated by a ZF region, as discussed in [18,19], which generates spatial intensity modulations on the detector, due to the gradient of magnetic field integrals across the devices. The intensity modulation can be used to measure the real-space density autocorrelation function of samples and for dark field imaging. To achieve a high resolution, an intensity modulation with a small period is always favorable, which can be achieved, for example, by separating the two prisms far apart. This

Please cite this article as: R. Dadisman, J. Shen, H. Feng et al., Design and characterization of zero magnetic field chambers for high efficiency neutron polarization transport, Nuclear Inst. and Methods in Physics Research, A (2019), https://doi.org/10.1016/j.nima.2019.05.092.

is where a ZF region is required to minimize unwanted phase accumulation and to preserve the neutron polarization vectors by minimizing the magnetic field along the path. We have also tried using two pairs of Helmholtz coils between two prisms to transport polarization with an additional magnetic field stepper in between to provide a field flip. But it requires additional effort to properly shield or compensate the stray field projected out by the Helmholtz coil.

For SEMSANS, the two Wollaston prisms are located at distances L_1 and L_2 from the detector, where $L_1 > L_2$, with the sample and analyzer after the precession devices. As discussed in detail in [18,19], to minimize the aberrations and maximize the contrast of the intensity modulation on the detector due to the effect of beam divergence, the magnetic fields in the prisms must satisfy,

$$B_1 L_1 = B_2 L_2 \tag{1}$$

The spin echo length is proportional to the difference between the magnetic fields, $\delta_z \propto (B_2 - B_1) = B_2(1 - L_2/L_1)$. From this it is clear that a long distance between the precession devices, i.e., a long ZF tube, will allow for longer spin echo lengths.

3.1. The design of the ZF tube

Since the sample, where scattering occurs, is located after the second prism, the ZF region can be provided by a straight, closed magnetic shielding ZF tube. In this case, to achieve a higher shielding factor, a two-layer mu metal cylindrical tube bolted to the windows of the mu metal surrounding the prisms is capable of reducing the background magnetic fields by several orders of magnitude. This is the general design which was optimized for this case, the apparatus shown in Fig. 7. Analytical solutions for the optimum spacing of two "infinitely" long, cylindrical magnetic shielding concentric shells exist and predict an optimum ratio of the outer to inner radius of $r_{outer} \approx \sqrt{3}\, r_{inner}$ [20]. The expense and size of the magnetic shielding materials justifies a study of the flatness of this optimization to determine a point of diminishing returns, and so simulations were implemented using COMSOL [21] and MagNet [15] to study the shielding as a function of the spacing between the inner and outer tubes in the "short" and "infinitely long" limits. A 2D planar model, equivalent to the "infinitely" long limit, was made in COMSOL, and agrees with the analytical model. A 3D model of a 0.5 m long shield was made using MagNet, and indicated the optimum was found at a slightly higher ratio than the analytical solution for an external field transverse to the longitudinal axis of the cylinders. Aside from the different geometries, each simulation software also utilized slightly different B–H curves to determine the permeability of mu metal, which changes the overall field attenuation. Collectively, these demonstrate that, for the inner diameter ZF tube under consideration, the optimization does not change dramatically for a very long or very short ZF tube.

The first datum on Fig. 6 is for the case where the outer layer touches the inner layer. As the gap increases, there is a very sharp increase in the magnetic field attenuation. With $r_{outer}/r_{inner} = 1.25$, 99.7% of the maximum attenuation gain with $r_{outer}/r_{inner} = \sqrt{3}$ is achieved, using an outer layer which is 28% smaller. From the perspective of portability and cost, the ratio $r_{outer}/r_{inner} = 1.25$ is a value point for an effective shield. As in the case of Section 2, the open ends of the ZF tube require compensation coils to minimize the stray axial field and the fringe fields from the prisms.

3.2. Polarization transport measurements of the ZF tube in SEMSANS

The experiment was conducted at beamline CG-1D [22] at the HFIR. 2 Å neutrons were polarized using a V-cavity supermirror upstream of the Wollaston prisms. As shown in Fig. 7, instead of using a single prism as an individual unit, a dual prism was used, which is equivalent to a single prism with current doubled due to the doubling of the magnetic field integral [7]. A 2.25 m long ZF tube connected the two

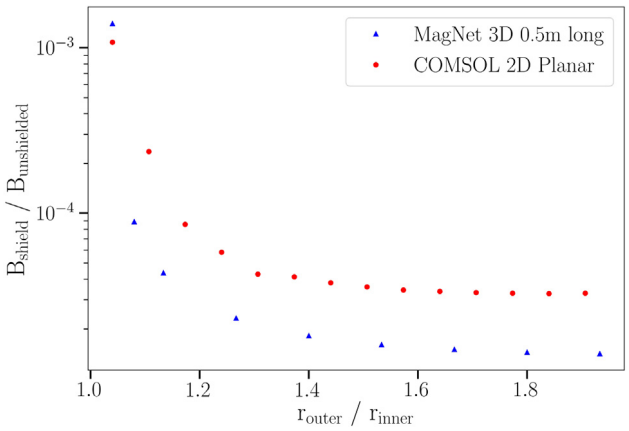

Fig. 6. Comparison of COMSOL and MagNet simulation results for magnetic field attenuation of a two-layer ZF tube demonstrates minimal improvement for $r_{outer}/r_{inner} > 1.25$.

prisms, and is constructed from 2-layers of 1.5 mm thick mu metal, radially separated by 10 mm and with an inner diameter of 75 mm. This corresponds to $r_{outer}/r_{inner} \approx 1.27$, near the ratio at which simulation indicates further attenuation gains are minimal. The tube flanges were directly bolted to the mu metal shielding of the prisms, as shown in Fig. 7. The flange overlaps with the prism shielding to reduce the magnetic field penetration into the otherwise open ends of the tubes, and a 20-turn compensation coil was wound on each end to further compensate the fringe fields. Downstream of the second prism was a ^{3}He spin analyzer and CCD detector, where are not shown in the picture.

In this case, the interior of the ZF tube cannot be accessed with a fluxgate, therefore, polarized neutrons are used as a probe to tune the compensation coils, as described before. For future routine operation, it would be advantageous to have fluxgates built into the design, which would save several hours from the compensation coil tuning procedure. However, as the Wollaston prisms are designed with flexibility to be used in a variety of setups, they do not have this built-in feature. The two arms were set to the same magnetic field and the two nutators aligned to produce a field parallel to the field inside the two arms. The left compensation coil was tuned by measuring the neutron polarization efficiency with the right coil turned off; the right coil was tuned by the same procedure, but with the left coil set at its optimum setting. Fig. 8 shows the optimization results for the left and right compensation coils. An interesting feature is that one of the compensation coils affects the polarization less than the other. There are two reasons for this: the right coil was tuned with the left coil off-tune, then the left coil was tuned with the right coil optimized; and there is a current imbalance inherent in the SEMSANS method as shown in Eq. (1), such that the field inside the right prism and thus the stray field requiring compensation is larger, a factor of three in this setup. At the optimized current settings $I_1 = 0.4$ A and $I_2 = -3.5$ A, the measured polarization was 79.4% without optimizing the experimental setup. For comparison, a measurement of the beam polarization using guide fields, rather than the ZF tube and Wollaston prisms apparatus, yielded a polarization efficiency of 89%. There is only 10% loss in polarization, which is acceptable considering a ZF tube of 2.25 m.

It is necessary to also determine whether any Larmor phase aberrations are generated through the ZF tube by measuring the spatial modulations of the polarization at the detector. After the compensation coils were tuned, the apparatus was set up for SEMSANS by setting the nutator fields perpendicular to the field inside the prisms ($\pi/2 - \pi/2$ mode). To maximize the contrast of the intensity modulations on the detector, the current inside the two arms were tuned to achieve $I_1 L_1 = I_2 L_2$, as in Eq. (1). Misalignment of prisms, guide fields, and detectors

Please cite this article as: R. Dadisman, J. Shen, H. Feng et al., Design and characterization of zero magnetic field chambers for high efficiency neutron polarization transport, Nuclear Inst. and Methods in Physics Research, A (2019), https://doi.org/10.1016/j.nima.2019.05.092.

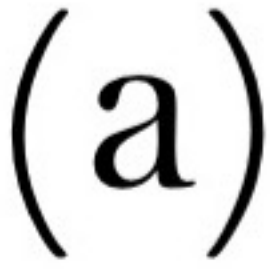

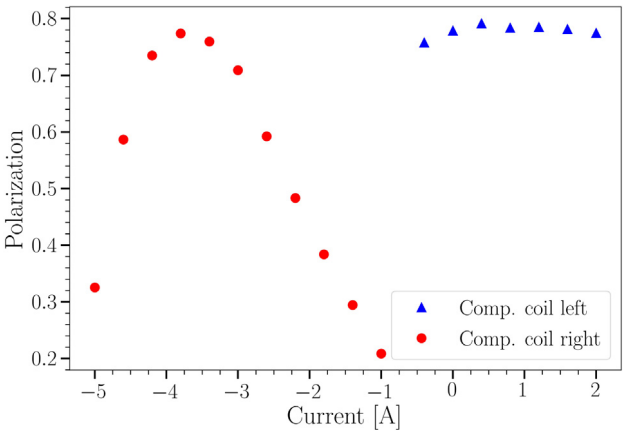

Fig. 8. The tuning curve of the left and right compensation coils by measuring the polarization transfer efficiency through the SEMSANS apparatus.

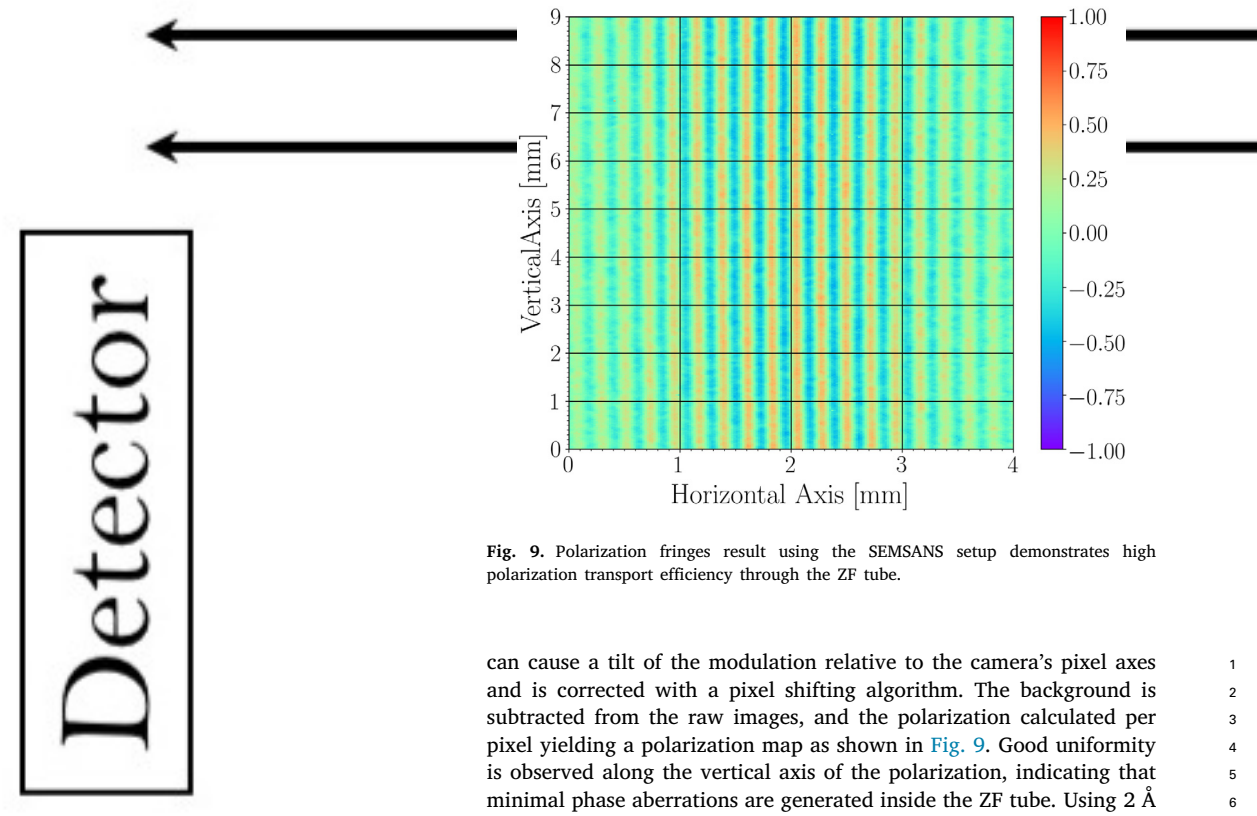

Fig. 9. Polarization fringes result using the SEMSANS setup demonstrates high polarization transport efficiency through the ZF tube.

can cause a tilt of the modulation relative to the camera's pixel axes and is corrected with a pixel shifting algorithm. The background is subtracted from the raw images, and the polarization calculated per pixel yielding a polarization map as shown in Fig. 9. Good uniformity is observed along the vertical axis of the polarization, indicating that minimal phase aberrations are generated inside the ZF tube. Using 2 Å neutrons, we measured a spatial period of 303 μm for prism currents I_1 = 14.59 A and I_2 = 4.59 A. Scaling this to the highest allowed current for the device (50 A), this same setup can achieve 88 μm. With cold neutrons, the fringe period can be further reduced.

4. Summary

We have presented the design of ZF chambers and discussed the operation and characterization of such chambers in combination with superconducting Wollaston prisms applied to both large angle and small angle polarized neutron scattering. Such techniques have the potential to be utilized for other polarized neutron scattering methods. We have demonstrated that a well designed ZF chamber is capable of achieving high efficiency polarization transport over long distances, 2.25 m in this work, which is important for high resolution neutron Larmor labeling techniques. For an apparatus in which the magnetic field flux is not well confined or the boundary not well defined, a ZF chamber might not be the best option [23]. Instead a homogeneous

guide field can be used to maintain polarization, with a flipper placed in the center such that phase aberrations caused by the guide field inhomogeneity may be minimized [6].

We have also presented a comparison of the compensation coil tuning methods for ZF chambers, using magnetometry and neutron polarization. Both methods are shown to produce equivalent polarization transport results, which shows the effectiveness of the using fluxgate magnetometer as the tuning tool. Between the two methods, the amount of time required to perform the tuning is the key difference between fluxgate and neutron polarization methods. Without using complicated automated system, it takes less than 0.5 min to optimize the compensation coils for a ZF chamber using the fluxgate magnetometer for each given prism current. For a routinely operated instrument, this whole procedure can be automated with for example a proportional integral derivative (PID) control system. Therefore whenever a configuration change is made, the system can automatically compensate the stray field of all ports simultaneously. Such a design would require the magnetometers to avoid the beam area. For comparison, using polarized neutrons, the measurements would take several minutes per each compensation coil setting, depending on the beam intensity and detector efficiency. Potentially it would take hours to complete the compensation procedure for all the current settings inside the prisms. And this procedure can only performed one by one, which will scale up the time required for multiple ZF ports. This method is also strongly dependent on the initial current used in each coil, such that the actual optimum may not even be easily found using neutron polarization measurements alone. So, the fluxgate magnetometer provides us with another quick but effective way of tuning the ZF chamber, by which the whole experiment can be much simplified.

Acknowledgments

This research used resources at the High Flux Isotope Reactor, a DOE Office of Science User Facility operated by the Oak Ridge National Laboratory. We would like to thank Jack Doskow with Indiana University for CAD model contributions, Thomas Keller for supporting the design of the ZF chamber, Matthew Pearson with ORNL for software development and assistance setting up power supplies, and Tianhao Wang with ORNL for providing polarization results for the V-cavity and ^{3}He analyzer performance on beamline CG-1D.

References

[1] F. Mezei, Neutron spin echo: A new concept in polarized thermal neutron techniques, Z. Phys. A 255 (2) (1972) 146–160, http://dx.doi.org/10.1007/BF01394523.
[2] R. Golub, R. Gähler, A neutron resonance spin echo spectrometer for quasi-elastic and inelastic scattering, Phys. Lett. A 123 (1) (1987) 43–48, http://dx.doi.org/10.1016/0375-9601(87)90760-2.
[3] R. Gähler, R. Golub, T. Keller, Neutron resonance spin echo—a new tool for high resolution spectroscopy, Physica B 180–181 (1992) 899–902, http://dx.doi.org/10.1016/0921-4526(92)90503-K.
[4] M. Rekveldt, Novel SANS instrument using neutron spin echo, Nucl. Instrum. Methods Phys. Res. B 114 (3) (1996) 366–370, http://dx.doi.org/10.1016/0168-583X(96)00213-3.
[5] W.G. Bouwman, C.P. Duif, J. Plomp, A. Wiedenmann, R. Gähler, Combined SANS–sesans, from 1nm to 0.1mm in one instrument, in: Proceedings of the 8th International Workshop on Polarised Neutrons for Condensed Matter Investigation, Physica B 406 (12) (2011) 2357–2360, http://dx.doi.org/10.1016/j.physb.2010.11.069.
[6] O. Uca, Spin-echo small-angle neutron scattering development, Ph.D. thesis, Delft University of Technology, 2003.
[7] F. Li, S.R. Parnell, W.A. Hamilton, B.B. Maranville, T. Wang, R. Semerad, D.V. Baxter, J.T. Cremer, R. Pynn, Superconducting magnetic wollaston prism for neutron spin encoding, Rev. Sci. Instrum. 85 (5) (2014) 053303, http://dx.doi.org/10.1063/1.4875984.
[8] F. Li, H. Feng, A.N. Thaler, S.R. Parnell, W.A. Hamilton, L. Crow, W. Yang, A.B. Jones, H. Bai, M. Matsuda, D.V. Baxter, T. Keller, J.A. Fernandez-Baca, R. Pynn, High resolution neutron larmor diffraction using superconducting magnetic wollaston prisms, Sci. Rep. 7 (1) (2017) 865.
[9] F. Li, H. Feng, A.N. Thaler, S.R. Parnell, L. Crow, M. Matsuda, F. Ye, T. Kimura, J.A. Fernandez-Baca, R. Pynn, New capabilities in high-resolution neutron larmor diffraction at ORNL, J. Appl. Crystallogr. 51 (3) (2018) 584–590.
[10] F. Li, R. Pynn, A novel neutron spin echo technique for measuring phonon linewidths using magnetic wollaston prisms, J. Appl. Crystallogr. 47 (6) (2014) 1849–1854.
[11] M. Janoschek, S. Klimko, R. Gähler, B. Roessli, P. Böni, Spherical neutron polarimetry with mupad, Physica B 397 (1) (2007) 125–130.
[12] T. Keller, B. Keimer, K. Habicht, R. Golub, F. Mezei, Neutron resonance spin echo-triple axis spectrometry (NRSE-TAS), in: Neutron Spin Echo Spectroscopy, in: Lecture Notes in Physics, Vol. 601, Springer Berlin Heidelberg, 2003, pp. 74–86.
[13] S. Klimko, Zeta, a zero field spin echo method for very high resolution study of elementary excitations and first application, Ph.D. thesis, Technische Universität Berlin, 2003.
[14] M. Duc Le, M. Skoulatos, D.L.a. Quintero-Castro, R. Toft-Petersen, F. Groitl, K.C. Rule, K. Habicht, The upgraded cold neutron three-axis spectrometer FLEXX at BER II at HZB, Neutron News 25 (2) (2014) 19–22.
[15] MagNet ©, Infolytica Corp.
[16] L. Crow, W.A. Hamilton, J.K. Zhao, J.L. Robertson, The HB-2d polarized neutron development beamline at the high flux isotope reactor, J. Phys. Conf. Ser. 746 (1) (2016) 012010.

Please cite this article as: R. Dadisman, J. Shen, H. Feng et al., Design and characterization of zero magnetic field chambers for high efficiency neutron polarization transport, Nuclear Inst. and Methods in Physics Research, A (2019), https://doi.org/10.1016/j.nima.2019.05.092.

[17] F. Mezei, Neutron spin echo and polarized neutrons, in: Inelastic Neutron Scattering, IAEA, Vienna, 1978, p. 125.
[18] F. Li, S.R. Parnell, H. Bai, W. Yang, W.A. Hamilton, B.B. Maranville, R. Ashkar, D.V. Baxter, J.T. Cremer, R. Pynn, Spin echo modulated small-angle neutron scattering using superconducting magnetic wollaston prisms, J. Appl. Crystallogr. 49 (2016) 55–63, http://dx.doi.org/10.1107/S1600576715021573.
[19] F. Li, S.R. Parnell, R. Dalgliesh, A. Washington, J. Plomp, R. Pynn, Data correction of intensity modulated small angle scattering, Scientific Reports 9 (1) (2019) http://dx.doi.org/10.1038/s41598-019-44493-9.
[20] V.V. Yashchuk, S.-K. Lee, E. Paperno, Magnetic shielding, in: Optical Magnetometry, Cambridge University Press, 2013, pp. 225–248, http://dx.doi.org/10.1017/CBO9780511846380.013.
[21] COMSOL Multiphysics ©, version 5.4, COMSOL Inc., URL www.comsol.com.
[22] L. Santodonato, H. Bilheux, B. Bailey, J. Bilheux, P. Nguyen, A. Tremsin, D. Selby, L. Walker, The CG-1D neutron imaging beamline at the oak ridge national laboratory high flux isotope reactor, in: Proceedings of the 10th World Conference on Neutron Radiography (WCNR-10) Grindelwald, Switzerland October 5–10, 2014, Physics Procedia 69 (2015) 104–108, http://dx.doi.org/10.1016/j.phpro.2015.07.015.
[23] J. Plomp, Spin-echo development for a time-of-flight neutron reflectometer, Ph.D. thesis, Delft University of Technology, 2009.

Please cite this article as: R. Dadisman, J. Shen, H. Feng et al., Design and characterization of zero magnetic field chambers for high efficiency neutron polarization transport, Nuclear Inst. and Methods in Physics Research, A (2019), https://doi.org/10.1016/j.nima.2019.05.092.